



Article

Feasibility of Bi-Temporal Airborne Laser Scanning Data in Detecting Species-Specific Individual Tree Crown Growth of Boreal Forests

Maryam Poorazimy ^{1,*}, Ghasem Ronoud ¹, Xiaowei Yu ², Ville Luoma ³, Juha Hyyppä ², Ninni Saarinen ¹, Ville Kankare ¹ and Mikko Vastaranta ¹

¹ School of Forest Sciences, University of Eastern Finland, 80101 Joensuu, Finland

² Department of Photogrammetry and Remote Sensing, Finnish Geospatial Research Institute, National Land Survey of Finland, 02430 Masala, Finland

³ Department of Forest Sciences, University of Helsinki, 00790 Helsinki, Finland

* Correspondence: maryam.poorazimy@uef.fi



Citation: Poorazimy, M.; Ronoud, G.; Yu, X.; Luoma, V.; Hyyppä, J.; Saarinen, N.; Kankare, V.; Vastaranta, M. Feasibility of Bi-Temporal Airborne Laser Scanning Data in Detecting Species-Specific Individual Tree Crown Growth of Boreal Forests. *Remote Sens.* **2022**, *14*, 4845. <https://doi.org/10.3390/rs14194845>

Academic Editors: Sandra Buján and Andrea Hevia

Received: 20 August 2022

Accepted: 21 September 2022

Published: 28 September 2022

Publisher's Note: MDPI stays neutral with regard to jurisdictional claims in published maps and institutional affiliations.



Copyright: © 2022 by the authors. Licensee MDPI, Basel, Switzerland. This article is an open access article distributed under the terms and conditions of the Creative Commons Attribution (CC BY) license (<https://creativecommons.org/licenses/by/4.0/>).

Abstract: The tree crown, with its functionality of assimilation, respiration, and transpiration, is a key forest ecosystem structure, resulting in high demand for characterizing tree crown structure and growth on a spatiotemporal scale. Airborne laser scanning (ALS) was found to be useful in measuring the structural properties associated with individual tree crowns. However, established ALS-assisted monitoring frameworks are still limited. The main objective of this study was to investigate the feasibility of detecting species-specific individual tree crown growth by means of airborne laser scanning (ALS) measurements in 2009 (T1) and 2014 (T2). Our study was conducted in southern Finland over 91 sample plots with a size of 32 × 32 m. The ALS crown metrics of width (WD), projection area (A_{2D}), volume (V), and surface area (A_{3D}) were derived for species-specific individually matched trees in T1 and T2. The Scots pine (*Pinus sylvestris*), Norway spruce (*Picea abies* (L.) H. Karst), and birch (*Betula* sp.) were the three species groups that studied. We found a high capability of bi-temporal ALS measurements in the detection of species-specific crown growth (Δ), especially for the 3D crown metrics of V and A_{3D} , with Cohen's D values of 1.09–1.46 (p -value < 0.0001). Scots pine was observed to have the highest relative crown growth ($r\Delta$) and showed statistically significant differences with Norway spruce and birch in terms of $r\Delta WD$, $r\Delta A_{2D}$, $r\Delta V$, and $r\Delta A_{3D}$ at a 95% confidence interval. Meanwhile, birch and Norway spruce had no statistically significant differences in $r\Delta WD$, $r\Delta V$, and $r\Delta A_{3D}$ (p -value < 0.0001). However, the amount of $r\Delta$ variability that could be explained by the species was only 2–5%. This revealed the complex nature of growth controlled by many biotic and abiotic factors other than species. Our results address the great potential of ALS data in crown growth detection that can be used for growth studies at large scales.

Keywords: LiDAR; growth and yield; monitoring; Scots pine; Norway spruce; birch; change detection

1. Introduction

Forests are long-lived dynamic biological systems that are continuously changing [1,2]. These changes occur in response to natural and anthropogenic disturbances, including internal growth, mortality, and forest management activities. Tree growth is a health indicator that closely relates to the forest structure. It reflects the terrestrial carbon cycle and changes in the soil nutrient cycling and global water–carbon balance [3]. Furthermore, there is a great interest in monitoring climate change's effects on forest growth [4]. Growth information plays a key role in sustainable management, allowing managers to assess the current forest structure and composition, as well as engage in long-term planning due to the ability to update field inventory data and predict future yields under different management alternatives [1,3]. This, in turn, has economic implications in a forest-dependent economy. However, growth models, especially at the individual tree-level, heavily relies on field

inventory data [5–7]. Individual tree-level growth models simulate each individual tree's growth as a basic unit, and the sum of the resulting estimates presents the stand growth values. The advantage of this method includes providing maximum detail and flexibility to evaluate different stand treatments [1,8]. In addition, crown structure as an essential part of tree growth in terms of assimilation, respiration, and transpiration can be incorporated into individual tree-level growth models [9]. It is a descriptor of the growth response to thinning and spacing [10]. Knowledge of the crown structure enhances our understanding of key forest ecosystem ecological aspects, including productivity, forest health, soil moisture availability, and biodiversity. However, crown dynamics have rarely been studied due to difficulties in obtaining suitable measurements [6]. Moreover, competition indices based on the crown structure as key inputs of many growth models are often obtained via an indirect relationship between the tree height and diameter. Consequently, this might introduce an uncertainty source into the growth analysis [5,11]. Hence, accurate and efficient crown growth estimating has become an issue to be addressed for precise forestry and sustainable management.

Repeated measurements on permanent sample plots are the most common way to achieve forest growth information, though it is labor-intensive and time-consuming to obtain usable datasets, especially for crown measures. Stem analysis is another approach that can provide long-term growth information, but it is destructive, expensive, and introduces uncertainty if the dominant sample trees selected as site trees have been dominant for their entire life [12,13]. These limitations were addressed using cost-effective remote sensing technologies as a comprehensive and accurate measure of forest change at different spatial scales [14]. Out of the current technologies, airborne laser scanning (ALS) data featured prominently when resolving 3D vegetation structure accurately [15–18]. The use and availability of ALS data are increasing rapidly given its proven capabilities, allowing for the study of forest ecosystem dynamics [19–22]. Although it is well documented, established ALS-assisted monitoring frameworks are still limited; thus, more case studies are required at different spatiotemporal scales and for diverse forest types [23–25]. On the other hand, ALS's potential was demonstrated in individual tree crown-based inventories [26–29]. For instance, Frew et al. [30] used the manual detection of individual trees to directly estimate tree height and crown metrics to determine the crown volume. This was based on field points of interest, discrete ALS datasets, and multispectral imagery. They concentrated on Douglas fir (*Pseudotsuga menziesii* [Mirb.] Franco var. *menziesii*) trees and found an R^2 of 0.45 in comparison to the field-measured crown volume. They also presented the estimation accuracy for different diameters at breast height (dbh) classes. In another study, Jung et al. [31] estimated the crown base height, volume, and area by means of ALS for 15 selected trees in Korean pine (*Pinus koraiensis*) stands. The regression analysis between the estimated results of the ALS and the one obtained using terrestrial laser scanning (TLS) as reference data resulted in R^2 values of 0.75, 0.69, and 0.58 for the mentioned metrics, respectively. Consequently, high demand has emerged for characterizing tree crown structures and their dynamics, stimulating attempts to link these measurements with conventional individual tree growth models [21,32]. However, growth studies using ALS data were mainly conducted at the level of a grid cell, i.e., a regular, fixed area spatial unit larger than tree crowns [33–38], while a few studies were conducted to detect individual tree crown growth [30,37,39]. On the other hand, tree responses to lightning conditions, growing space, and resources vary between tree species. This means that tree growth is prone to high variability between tree species as an intrinsic source of change [40,41]. Therefore, the main objective of this study was to investigate the feasibility of bi-temporal ALS data in detecting species-specific individual tree crown growth. They were used to estimate the species-specific crown growth metrics of width (WD), projection area (A_{2D}), volume (V), and surface area (A_{3D}) at the individual tree-level for three species groups: Scots pine (*Pinus sylvestris*), Norway spruce (*Picea abies* (L.) H. Karst), and birch (*Betula* sp.). Our specific research questions were as follows: (1) Are the ALS-derived crown metrics of WD, A_{2D} , V, and A_{3D} affected by growth (Δ) over a 5-year time interval? (2) How does relative growth

($r\Delta$) in the mentioned metrics differ between tree species groups? Our results provide an insight into how tree species differ in their life history strategies in terms of resource acquisition, defense against natural enemies, and allocation to reproduction.

2. Materials and Methods

2.1. Site Description and Field Data

This study was conducted in Evo (61.19°N, 25.11°E), southern Finland, and included approximately 2000 ha of managed Boreal forests (Figure 1a). The study area elevation ranged from 125 m to 185 m above sea level and the stands were mainly even-aged and single layer, with an average stand size of slightly less than 1 ha. Scots pine, Norway spruce, and birch were the dominant tree species in the study area, contributing 44.7%, 33.5%, and 21.8% of the total volume, respectively.

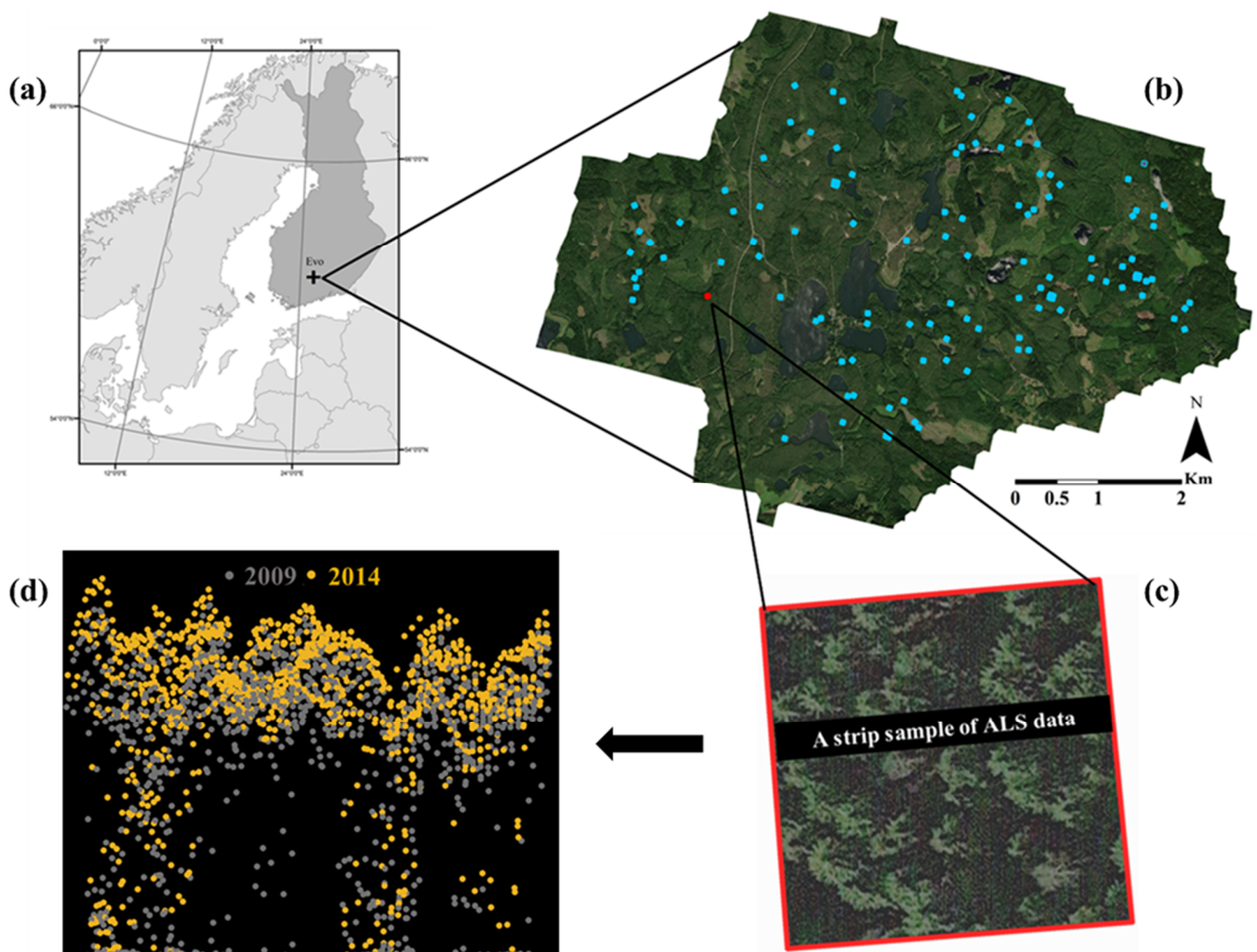


Figure 1. (a) Study area in Evo, Finland, and (b) distribution of the field plots. (c) A strip sample of a plot showing the bi-temporal ALS data acquired in 2009 (gray) and 2014 (yellow) (d).

A total of 91 rectangular sample plots with an area of 1024 m² were used in this study (Figure 1b). They were established in 2014 to represent a wide range of forest structural conditions [42]. For each sample plot, an initial tree map was created based on the TLS data. Tree maps were verified during the field measurements. All trees with a diameter at breast height (dbh) of at least 5 cm were measured for their dbh with a caliper and height with a Vertex IV (Haglöf Sweden AB, Långsele, Sweden). The health status and tree species were also determined for each measured tree on site. They were used to compute the tree-level basal area by considering the cross-sectional area of a tree to be circular and

the stem volume using the nationwide species-specific volume equation [43]. The sum and basal-area-weighted mean descriptive statistics of the field plots are presented in Table 1.

Table 1. Descriptive statistics of the field plots. The minimum (Min), maximum (Max), Mean, and standard deviation (S.D.) of the number of trees, mean volume, basal-area-weighted mean diameter, and basal-area-weighted height are reported.

Attribute	Min	Max	Mean	S.D.
Number of trees ($n \text{ ha}^{-1}$)	342	3076	943	556
Mean volume ($\text{m}^3 \text{ ha}^{-1}$)	34.46	518.39	271.49	110.73
Basal-area-weighted mean dbh (cm)	13.91	46.42	25.79	7.51
Basal-area-weighted mean height (m)	10.02	31.09	21.10	4.42

2.2. Airborne Laser Scanning Data

Georeferenced bi-temporal ALS data were collected in 2009 (T1) and 2014 (T2) across the study area under leaf-on canopy conditions (Figure 1d). Leica ALS-50II SN058 in T1 and 70HA in T2 were used for collecting the ALS data. The acquisition specifications are listed in Table 2. The T1 dataset had the highest sampling density with an average nominal density of 10 pulses/ m^2 , followed by 6 pulses/ m^2 for the T2 dataset, recording between 3 and 5 discrete returns per pulse.

Table 2. The 2009 and 2014 ALS datasets and acquisition specifications.

Year	2009	2014
Sensor	Leica ALS50II SN058	Leica ALS70-HA
Date	25 July 2009	5 September 2014
Laser pulse frequency	150,000 kHz	240 kHz
Scan frequency	52.2 Hz	59.90 Hz
Beam divergence	0.22 mrad	0.15 mrad
Flying altitude	400 m	900 m
Scanning angle	30°	30°
Average pulse density	10	6

2.3. Establishing a Monitoring Framework at the Individual Tree-Level

The objective of this section is to describe the applied framework for estimating individual tree crown growth with the assistance of ALS data. An overview of the methodologies used is depicted in Figure 2. We implemented a set of ALS data processing steps to obtain a canopy height model (CHM) and detect individual trees using marker-controlled watershed segmentation (Section 2.3.1). Then, species-specific tree-to-tree matching was implemented using both the tree locations and their segments (Section 2.3.2). The 2D and 3D convex hull algorithms were applied to extract the crown metrics of width (WD), projection area (A_{2D}), volume (V), and surface area (A_{3D}) (Section 2.3.3). Finally, the ALS-derived crown changes of the tree species groups were statistically evaluated to determine whether they were affected by growth over a 5-year time interval and how they differed between tree species groups (Section 2.3.4).

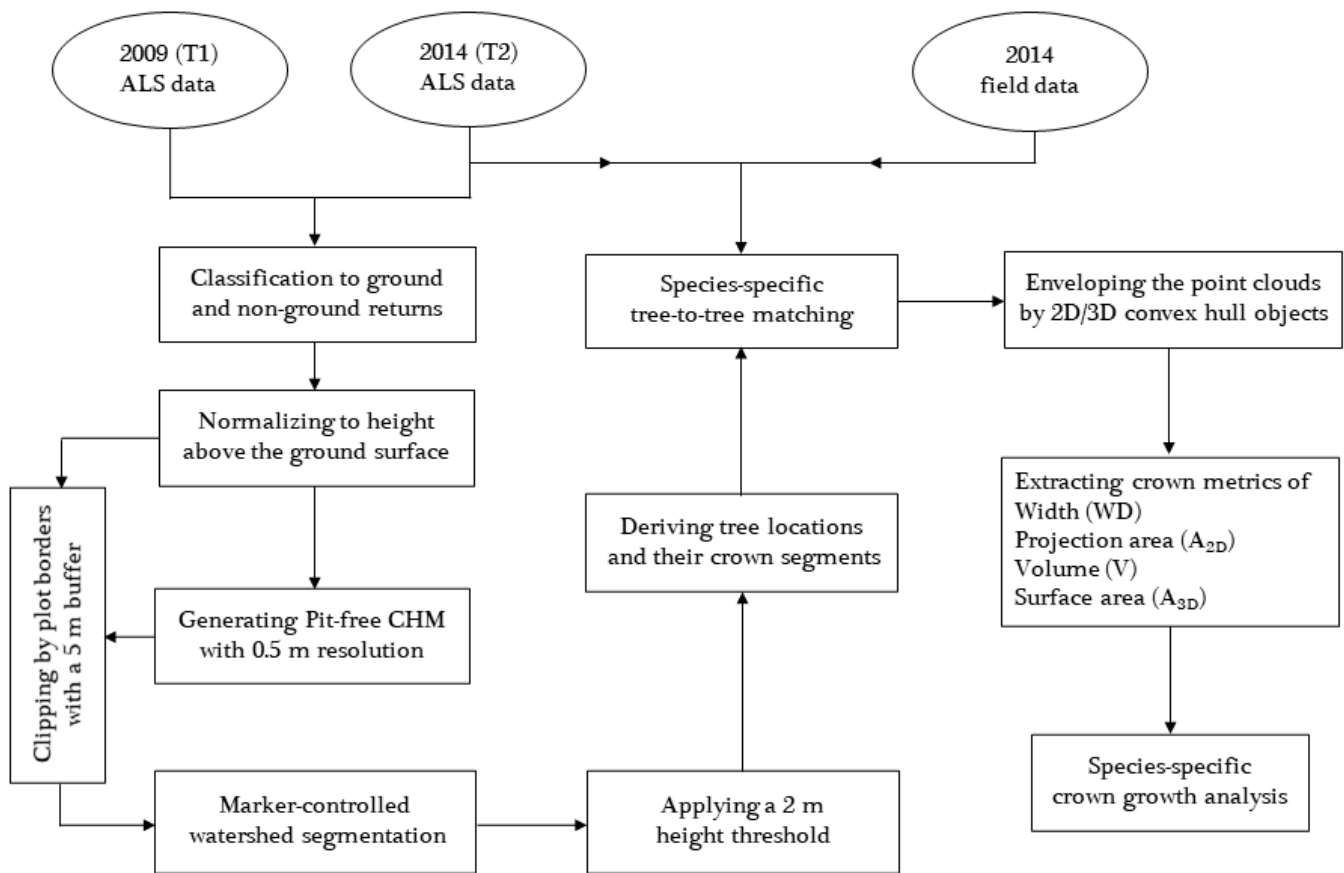


Figure 2. Flowchart of the established monitoring framework.

2.3.1. Bi-Temporal ALS Data Processing

The ALS point clouds were classified into ground and non-ground returns using TerraScan software. This was done based on the triangular irregular network (TIN) method developed by Axelsson [44]. The lasheight tool from LAStools software was further used to normalize the point cloud elevations, i.e., the Z-coordinate relative to the height above the ground surface. The whole process was assisted by creating 3000×3000 m tiles with a 20 m buffer to avoid edge effects [45].

The pit-free algorithm introduced by Khosravipour et al. [46] was used to generate the CHMs in the LAStools software (Figure 3a). The algorithm works based on a standard CHM and partial CHMs generated from all and the highest return ALS points close to the pits, respectively. In our study, a set of increasing height thresholds of 2, 5, 10, 15, . . . , 40 m were used to obtain the partial CHMs. They were generated using normalized point cloud data that were thinned with half of the pixel size instead of all first returns. In addition, we included a ground CHM by excluding the normalized point clouds above 0.1 m to fill potential holes [47]. Then, all points were combined in a pixel size of 0.5 m based on the highest value across all points. The same process was applied to both the T1 and T2 ALS datasets to obtain pit-free CHMs. Finally, they were clipped using field plot polygons, which were buffered by 5 m to avoid boundary effects. The T1 CHM of the whole study area and its zoomed-in views are shown in Figure 3b,c, respectively.

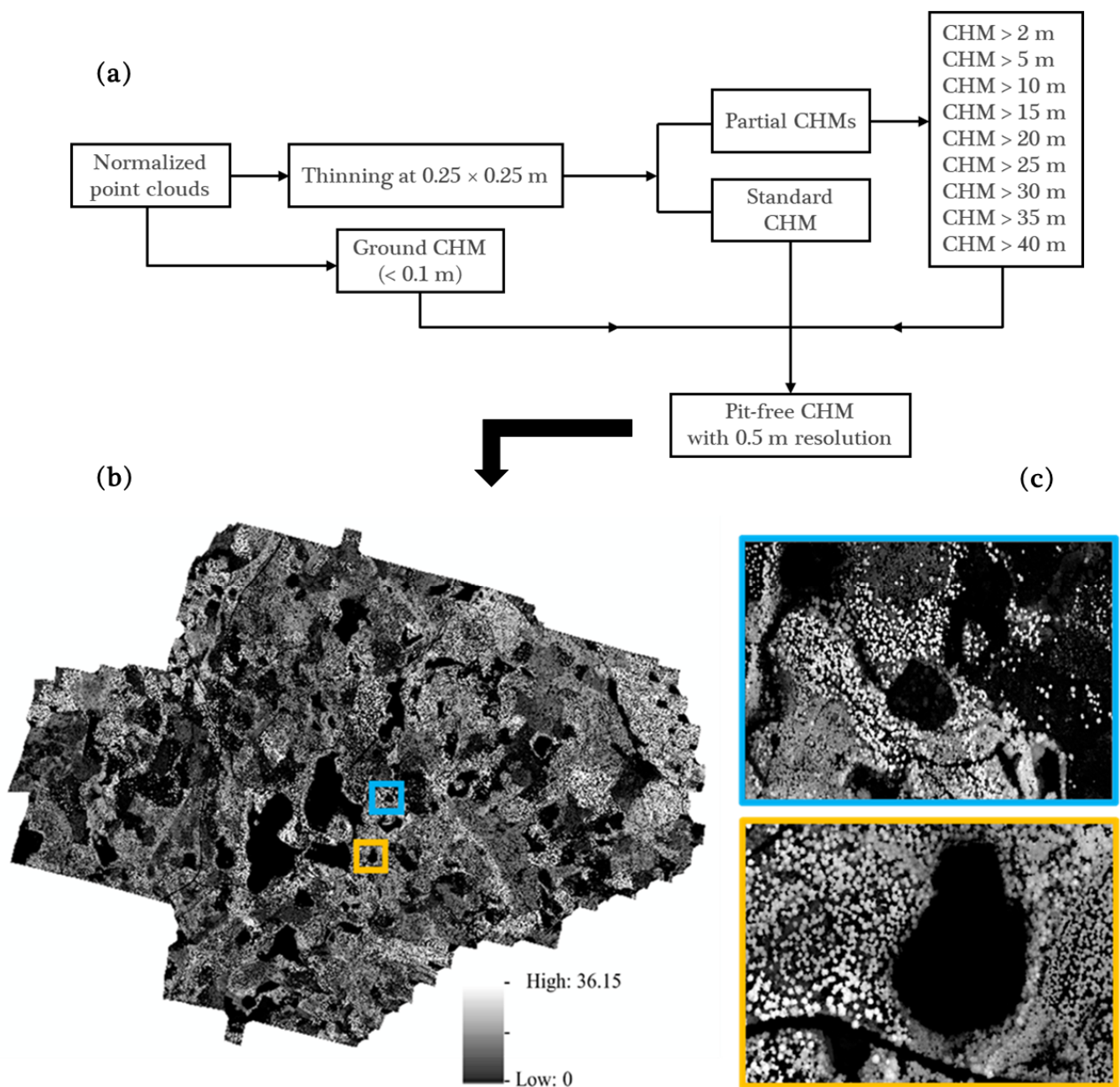


Figure 3. (a) Pit-free algorithm, (b) canopy height model (CHM) of the whole study area in T1 (2009), and (c) its zoomed-in views.

To conduct the analysis at the individual tree-level, a local maxima filter (LMF) was applied to the CHMs to find the treetops. This was carried out in the lidR package of R [48] with an experimentally checked fixed window size of 3×3 pixels. Then, they were treated as markers for the watershed algorithm to delineate crown segments, analogous to pouring water into the inverted CHM [49]. Identical processes were applied to both the T1 and T2 datasets. The generated crown segments were used to clip out the normalized point cloud data that fell within them for further extraction of the tree location and canopy metrics. In this study, the location of each tree was defined based on the planar location of the highest point within each crown segment. Notably, we excluded points belonging to the understory vegetation and shrubs using a 2 m height threshold [50].

2.3.2. Species-Specific Tree-to-Tree Matching

Tree-to-tree matching is an important aspect of individual tree-level growth analysis [51]. Tree locations and/or their crown segments can be utilized in the matching process. As many studies presenting individual tree-level growth analysis concentrate on height, the matching was applied to the 2D or 3D distance between tree locations at different times [36,52,53]. In this study, species-specific tree-to-tree matching was applied based on using both individual tree locations and their crown segments. This process was done in two steps using the spatial join tools of ArcGIS software [54]. First, we matched T2 ALS trees and field data to obtain tree species information, as they were collected at the same time. Considering the reduction in the tree detection rate for the co-dominant, intermediate, and suppressed trees using ALS data, the small understory trees of the field data were excluded from the analysis [55,56]. Therefore, the polygons of the T2 ALS crown segments were matched with the locations of the highest field-measured trees of the dominant layer within those polygons, extracting tree species information for the T2 ALS dataset.

Second, polygons of the T2 ALS crown segments were overlaid with the T1 ALS tree locations and vice versa. Because of the possible differences in segmentation accuracy of the T1 and T2 due to their point densities, over- and undersegmentation errors were identified. To ensure proper growth analysis, the polygons of the T2 ALS crown segments that contained only one tree location of T1 ALS were kept and vice versa, eliminating the commission errors. We also kept those matched trees that existed in both T1 and T2 and did not show a decrease in height by a threshold of 3 m. These heuristic rules were introduced, as some trees had disappeared during the 5-year time interval due to mortality, logging, and damage. Similarly, the tree heights of live trees should not have decreased.

The proposed method was assumed to be a compensation for the possible spatial mismatch between tree locations caused by ALS acquisition discrepancies and prevailing wind patterns at the acquisition time. Matched trees were further classified based on their field-measured species into the three groups of Scots pine, Norway spruce, and birch. Considering the effect of outliers on the probability of a type II error by decreasing the power [57], we removed each species-specific crown metric that was three times the inter-quartile range larger than the first and third quartile, resulting in sample sizes of 947, 749, and 402 for the Scots pine, Norway spruce, and birch, respectively. Species-specific descriptive statistics of the matched trees that were measured in field plots at T2 are presented in Table 3.

Table 3. Field-measured species-specific descriptive statistics of the matched trees at T2. The Mean and standard deviation (S.D.) values of the diameter at breast height (dbh), volume, and height are reported.

Species Group	Diameter at Breast Height (cm)		Volume (m ³)		Height (m)	
	Mean	S.D.	Mean	S.D.	Mean	S.D.
Scots pine (n = 947)	21.74	6.77	0.41	0.36	19.65	4.27
Norway spruce (n = 749)	20.42	10.37	0.46	0.50	22.09	5.66
Birch (n = 402)	15.73	6.46	0.22	0.24	19.71	4.10

2.3.3. Extracting Canopy Metrics

The crown structure for the species-specific matched trees of T1 and T2 was characterized using geometrical descriptors based on 2D and 3D convex hulls [58,59]. Four crown metrics were extracted as follows using the rLiDAR package of R [60]. The crown width (WD), which is the distance between the two most outer points in xy space, and the projection area (A_{2D}) were obtained by identifying the crown point clouds lying on the 2D

convex hull. Meanwhile, the crown volume (V) and surface area (A_{3D}) were computed using a 3D convex hull by applying Delaunay triangulations to the outer points of the closed convex surface boundary [58]. Figure 4 exhibits an example of species-specific matched trees with their crown metrics derived at T1 and T2.

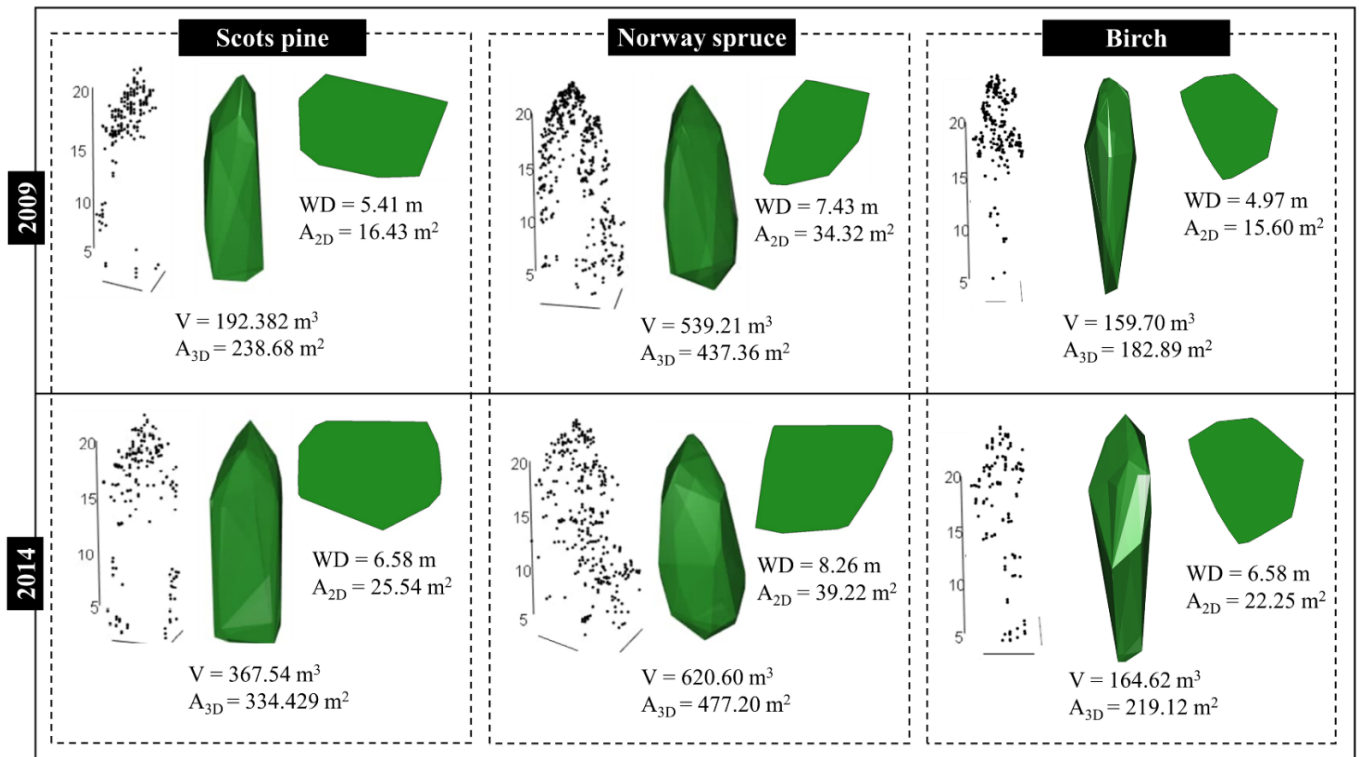


Figure 4. Illustration of species-specific ALS-derived crown metrics in T1 (2009) and the respective measures in T2 (2014). WD, A_{2D} , V , and A_{3D} are crown width, projection area, volume, and surface area, respectively.

The consistency of the ALS-derived crown metrics in T1 and T2 was analyzed using Pearson's correlation coefficient (Figure 5). A strong correlation was found for the T1 and T2 crown metrics of A_{2D} , V , and A_{3D} in Norway spruce, followed by birch and Scots pine ($R = 0.86$ – 0.94). In comparison, the extracted WD at T1 and T2 resulted in lower correlations of 0.80 for Norway spruce, 0.77 for birch, and 0.70 for Scots pine. It can be concluded that the crown metrics of all tree species displayed repeated consistency over the 5-year time interval.

2.3.4. Crown Growth Estimation and Statistical Analysis

The crown growth (Δ) was obtained by subtracting the crown metrics at T1 from their respective measure at T2. The relative crown growth ($r\Delta$) was also computed by dividing the obtained growth from the measure estimated at T1 to minimize the inherent differences in scale between different trees [61]. To evaluate the species-specific statistically significant differences in the means of WD, A_{2D} , V , and A_{3D} during the 5-year time interval, the paired t -test was used, i.e., a within-group test using the `rstatix` package of R. Although based on the central limit theorem, we can assume that the sample means came from a normal distribution, it did not guarantee the normal distribution of the population [62]. In addition, in our skewed datasets of A_{2D} , V , and A_{3D} , the median is a better measure of central tendency than the mean (see the marginal histograms in Figure 5) [63]. Therefore, the data were also compared with the Wilcoxon signed-rank test.

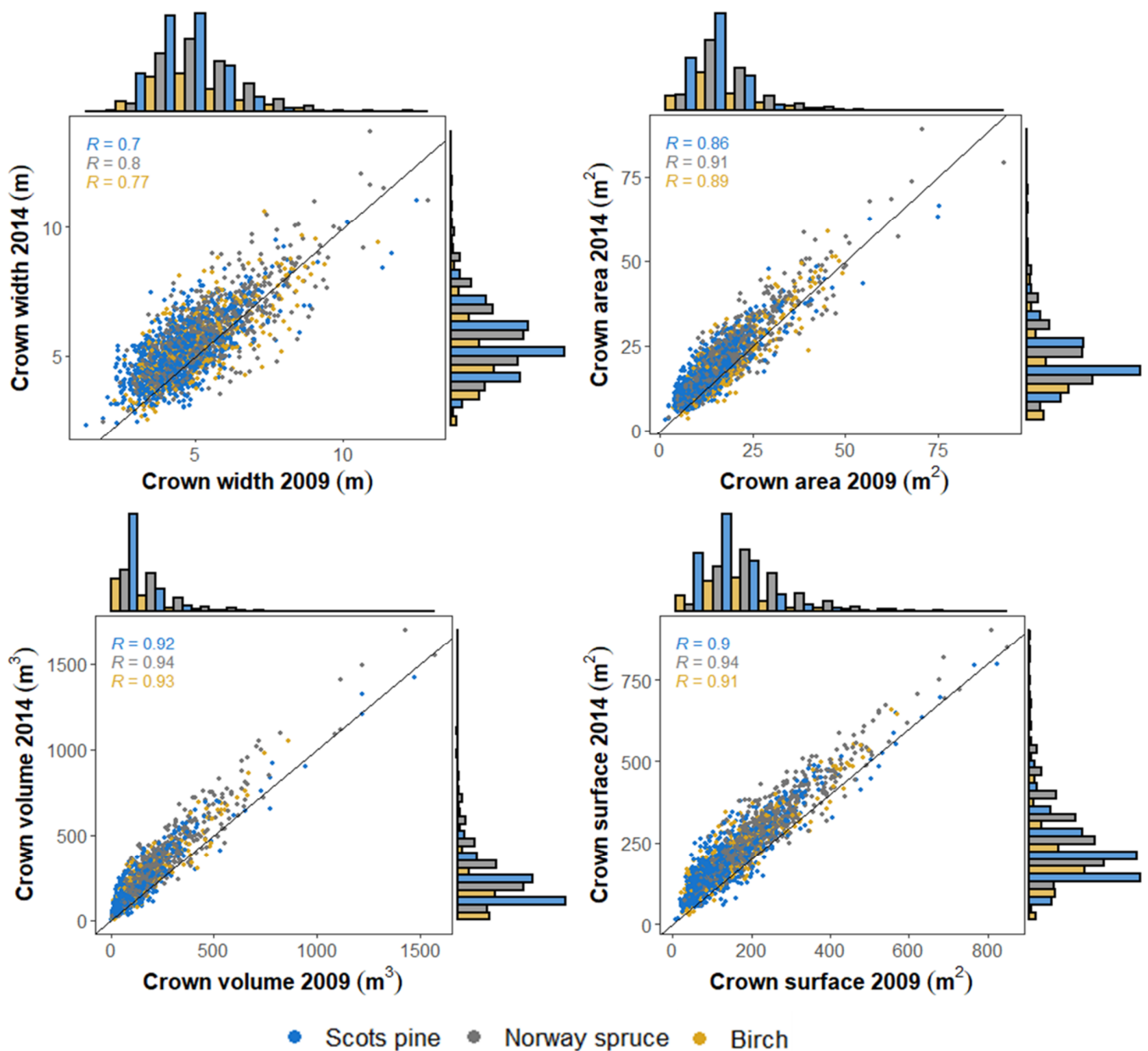


Figure 5. Consistency of ALS-derived species-specific crown metrics in T1 (2009) and T2 (2014).

Welch ANOVA/Kruskal–Wallis and pairwise comparisons were further applied to compare the $r\Delta_{WD}$, $r\Delta_{A_{2D}}$, $r\Delta_V$, and $r\Delta_{A_{3D}}$ between different species groups, i.e., between groups. As the significance level (p -value) strongly depends on the sample size, the effect size was also investigated to measure the strengths of the effects. The effect sizes of Cohen's D as the mean difference and generalized eta squared (η^2) as the explained variance were used [64,65]. To interpret the results, we used the following rules of thumb: Cohen's D of 0.2, 0.5, and 0.8, and η^2 values of 0.01, 0.06, and 0.14 denoted a weak, medium, and large effect size, respectively. We applied Bonferroni correction to control the probability of committing a type I error. Thus, the p -values were multiplied by the number of comparisons [63].

3. Results

3.1. Crown Growth Detection within Different Species Groups

Based on the paired t -test, all mean differences in the ALS-derived WD , A_{2D} , V , and A_{3D} at T1 and T2 were found to have increased significantly with a p -value < 0.0001 (Table 4). This meant that a significant Δ occurred during the 5-year monitoring period, which was

detectable using the ALS data at a 95% confidence interval. Overall, Δ WD and ΔA_{2D} were estimated to be 0.47 m (standard deviation (S.D.) of 0.92 m) and 3.13 m² (S.D. of 4.19 m²), respectively. It was 70.80 m³ for ΔV with an S.D. of 62.28 m³ and 55.49 m² for ΔA_{3D} with an S.D. of 41.64 m².

Table 4. T1 (2009) and T2 (2014) ALS-derived crown metrics of width (WD), projection area (A_{2D}), volume (V), and surface area (A_{3D}), and their growth (Δ). The Mean, standard deviation (S.D.), and effect size (Cohen's D) values are reported.

Species Group	Metrics	T1		T2		Δ		Cohen's D
		Mean	S.D.	Mean	S.D.	Mean	S.D.	
Scots pine (n = 947)	WD	4.56	1.20	5.12	1.14	0.56 ****	0.90	0.62
	A_{2D}	14.00	7.34	17.57	7.35	3.57 ****	3.85	0.93
	V	106.84	120.76	168.75	137.07	61.90 ****	54.26	1.14
Norway spruce (n = 749)	A_{3D}	136.45	90.02	189.62	94.94	53.17 ****	41.63	1.28
	WD	5.30	1.45	5.75	1.46	0.45 ****	0.91	0.50
	A_{2D}	18.82	9.73	22.09	10.35	3.27 ****	4.37	0.75
Birch (n = 402)	V	199.53	166.32	285.83	199.53	86.30 ****	70.64	1.22
	A_{3D}	215.76	108.30	276.21	117.73	60.44 ****	41.48	1.46
	WD	5.04	1.43	5.35	1.39	0.30 ****	0.96	0.32
All trees (n = 2098)	A_{2D}	17.27	9.07	19.08	9.58	1.81 ****	4.35	0.42
	V	147.78	132.07	210.64	156.86	62.86 ****	57.73	1.09
	A_{3D}	168.40	96.96	220.14	101.25	51.73 ****	41.20	1.26
All trees (n = 2098)	WD	4.92	1.38	5.39	1.34	0.47 ****	0.92	0.51
	A_{2D}	16.35	8.86	19.47	9.18	3.13 ****	4.19	0.75
	V	147.78	146.61	218.58	173.58	70.80 ****	62.28	1.14
All trees (n = 2098)	A_{3D}	170.89	104.37	226.38	111.69	55.49 ****	41.64	1.33

**** p -value < 0.0001.

Within different species groups, the estimated crown metrics at T1 were significantly different from the respective estimates at T2 (p -value < 0.0001). The observed Δ WD ranged from 0.30 to 0.56 m and were classified using Cohen's D of 0.32–0.62, i.e., small to medium effect size over all three different species groups. The estimated ΔA_{2D} differed by 0.93 and 0.75 times the S.D. in Scots pine and Norway spruce, respectively, while it was smaller for birch, i.e., 0.42. A maximum ΔA_{2D} of 3.57 m² was found for Scots pine. The observed ΔV values were 86.30, 62.86, and 61.90 m³ for Norway spruce, birch, and Scots pine, respectively. ΔA_{3D} showed a range of 51.73 to 60.44 m². The Cohen's D values for ΔV and ΔA_{3D} detected using ALS data were the highest for all three species groups, ranging from 1.09 to 1.22 and 1.26 to 1.46, respectively. The results of the Wilcoxon signed-rank test also indicated a statistically significant difference in the crown metric medians at T1 and T2. Therefore, only the t-test results are reported.

3.2. Relative Crown Growth Changes between Different Species Groups

The results of the Welch-ANOVA indicated that the means of $r\Delta$ WD differed significantly between the species groups (p -value < 0.0001). The maximum $r\Delta$ WD was observed for Scots pine (15.38 ± 23.30%), while Norway spruce and birch showed smaller increments (10.50% and 8.54%, respectively) (Table 5). The pairwise t-test comparison between species groups showed a statistically significant difference in $r\Delta$ WD for Scots pine–birch and Scots pine–Norway spruce (p -value < 0.0001). There was no statistically significant change for Norway spruce–birch regarding $r\Delta$ WD (Figure 6).

Table 5. Species-specific relative growth ($r\Delta$) of ALS-derived crown metrics of width (WD), projection area (A_{2D}), volume (V), and surface area (A_{3D}) in T1 (2009) and T2 (2014). The Mean, standard deviation (S.D.), p -value, and generalized eta squared effect size (η^2) values are reported.

Species Group	Metrics	$r\Delta$ (%)		p -Value	η^2
		Mean	S.D.		
WD	Scots pine	15.38	23.30	2.18×10^{-8}	0.02
	Norway spruce	10.50	18.50		
	Birch	8.54	20.89		
A_{2D}	Scots pine	35.42	41.05	2.4×10^{-22}	0.05
	Norway spruce	21.96	26.98		
	Birch	15.64	32.16		
V	Scots pine	97.67	94.77	1.93×10^{-16}	0.03
	Norway spruce	58.21	48.32		
	Birch	74.97	96.86		
A_{3D}	Scots pine	55.80	53.48	1.73×10^{-19}	0.04
	Norway spruce	34.14	27.24		
	Birch	46.89	58.91		

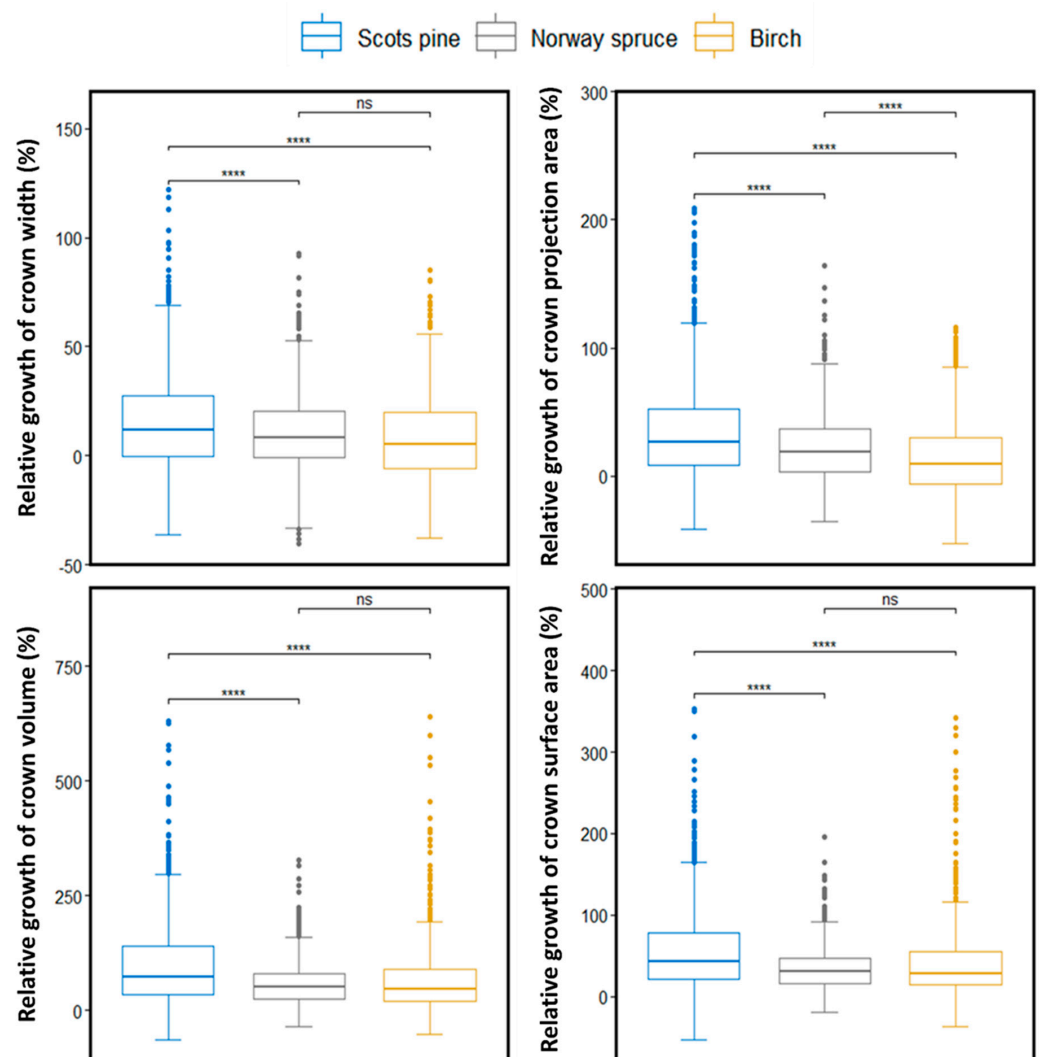


Figure 6. Pairwise comparisons of the relative growth (%) between different species groups. **** and ns (not significant) denote p -value < 0.0001 and > 0.05 , respectively.

Using the Kruskal–Wallis test, a statistically significant difference was also found between the medians of $r\Delta A_{2D}$, $r\Delta V$, and $r\Delta A_{3D}$ of the species groups (Table 5). Birch had the lowest $r\Delta A_{2D}$ of 15.64% with an S.D. of 32.16% during the monitoring period. The highest $r\Delta V$ was estimated for Scots pine (97.67%), followed by birch (74.97%) and Norway spruce (58.21%). Similarly, $r\Delta A_{3D}$ was the highest for Scots pine (55.80%) and the lowest for birch (46.89%) (Table 5). The pairwise Wilcoxon test revealed a similar magnitude of median differences in $r\Delta V$ and $r\Delta A_{3D}$ for Norway spruce–birch, while they statistically differed for Scots pine–Norway spruce and Scots pine–birch (Figure 6). Unlike with $r\Delta WD$, $r\Delta A_{2D}$ exhibited a significant difference in Norway spruce–birch (p -value < 0.0001). On average, the estimated $r\Delta WD$, $r\Delta A_{2D}$, $r\Delta V$, and $r\Delta A_{3D}$ of Norway spruce had lower S.D. values than other species, ranging from 18.50 to 48.32%. The highest variability was obtained for the $r\Delta A_{3D}$ and $r\Delta V$ of birch (S.D. of 58.91% to 96.86%) and the $r\Delta WD$ and $r\Delta A_{2D}$ of Scots pine (S.D. of 23.30% to 41.05%). Consequently, η^2 demonstrated a moderate proportion of $r\Delta A_{2D}$ variability that could be explained by the species (0.05). Moreover, it was 0.04, 0.03, and 0.02 for $r\Delta A_{3D}$, $r\Delta V$, and $r\Delta WD$, respectively (Table 5).

4. Discussion

Our main objective was to investigate the feasibility of bi-temporal ALS data in detecting crown growth over a 5-year time interval. The results showed that statistically significant ΔWD , ΔA_{2D} , ΔV , and ΔA_{3D} values were detected from the ALS data (p -value < 0.0001). A very large difference was obtained for the ΔA_{3D} of Norway spruce, followed by Scots pine and birch with Cohen's D values of 1.46, 1.28, and 1.26, respectively. The same trend was estimated for ΔV as large to very large effect sizes of 1.22, 1.14, and 1.09, respectively. This meant that the growth in the 3D crown metrics of V and A_{3D} could be effectively estimated using ALS data and further used in growth research (Table 4). The consistency of the ALS-derived A_{3D} and V in T1 and T2 was also the highest among the metrics ($R > 0.9$) (Figure 5). Therefore, they are reasonable metrics that might be useful in predicting the dbh, stem taper, and volume [30]. For instance, Yrttimaa et al. [59] demonstrated a strong correlation between the basal area growth and the attributes that characterize the crown structure and competition using terrestrial laser scanning data in boreal forests. The highest $r\Delta WD$, $r\Delta A_{2D}$, $r\Delta V$, and $r\Delta A_{3D}$ values were observed for Scots pine, i.e., 15.38%, 35.42%, 97.67%, and 55.80%, respectively. Of importance, they showed a significant difference with the other species groups of birch and Norway spruce with p -values < 0.0001 (Table 5). Despite the higher $r\Delta V$ and $r\Delta A_{3D}$ values of birch relative to Norway spruce, their mean changes were not statistically significant at a 95% confidence interval. Regarding the 2D crown metrics of ΔWD and ΔA_{2D} , the effect size of the observed change was higher for Scots pine than Norway spruce, i.e., 0.93 and 0.62, respectively. Furthermore, birch resulted in the lowest effect size of changes for ΔWD (0.32) and ΔA_{2D} (0.42) among the species (Table 4). This corresponded with the lowest $r\Delta WD$ and $r\Delta A_{2D}$ of birch relative to other species in the monitoring period. As shown in Table 3, the mean dbh of the birch sample trees measured at T2 (15.73 cm) was the lowest in comparison with Scots pine (21.74 cm) and Norway spruce (20.42 cm), which can be explained by the lower 2D crown growth of birch. Ma et al. [37] also observed a lower growth in crown area than in volume in coniferous-dominated stands. However, overlapping between the broad-leaved subject tree and the surrounding trees could lead to an underestimation of the crown width, especially considering the presence of birch in the dominant layer height (Table 3). This effect was related to tree density and would be increased by a reduced growing space [31,66]. Generally, coniferous trees are less flexible while developing and have a lower ability to close gaps [67]. However, our results showed that the observed $r\Delta WD$ values of birch and Norway spruce had no statistically significant difference, which partially corresponded with the results obtained by Vepakomma et al. [68].

On average, the estimated $r\Delta$ of crown metrics during the 5-year time interval showed a statistically significant difference between the species groups, but only 2–5% percent of these relationships could be explained by the species. One of the reasons could be the

high variation of $r\Delta$ among each species group, which was highest for V (48.32–96.86%), followed by A_{3D} (27.24–58.91%) (Table 5). This meant that except for the species, the tree size or age, stem density, and competition as biotic factors and soil nutrient level, local climate, topography, and water balance as abiotic factors controlled the growth [41,69]. Our findings corresponded to previous research on the impact of the mentioned internal tree competitiveness and external tree competition on individual tree growth [6,70,71]. However, we found a lower variation in $r\Delta_{WD}$ and $r\Delta_{A_{2D}}$, ranging from 18.50–23.30% and 26.98–41.05%, respectively. In our study area, the species-specific individual trees' responses to abiotic controlling factors of growth were probably allocating crown growth more to volume than horizontal elongation, as the highest $r\Delta$ was observed for 3D crown metrics.

Even though change detection at the individual tree-level provides detailed information, it suffers from additional challenges and uncertainties. Reliable change detection at an individual tree-level cannot be applied when the point density is low [36], and the success is largely dependent on the segmentation accuracy and attribute estimation [72]. In addition, time-series ALS measurements themselves can be biased because of the inconsistency in instrument specification, sampling rate, flight pattern, and weather conditions [13,20,36,73]. Hence, more studies are needed to determine the appropriate design for ALS time series measurements [34]. However, Zhao et al. [36] demonstrated no difference in growth analysis at the tree-level if the datasets have densities that exceed 7 pulses/m². On the other hand, we should consider that a higher pulse repetition frequency does not guarantee a higher accuracy, especially for an area-based approach [74–76]. This could be a crucial finding since modern ALS systems have point densities that are higher than a decade ago. Although a typically 5-year time interval was found to be enough to present the average level of growth and models predicting growth in boreal conditions [77,78], understanding the amount of time necessary to overcome excess noise and other ALS system uncertainties is still challenging [3,13,77]. It should be noted that the results of growth estimation using ALS data for individual trees could not correspond to the average growth in multi-layered forest stands since it is weighted by the dominant trees.

5. Conclusions

The crown structure as an essential part of growth is rarely studied because of the difficulty in conducting field measurements. Consequently, the crown-based competition indices as the main input of many growth models are commonly estimated via indirect regression models of tree height and dbh with the associated uncertainty. To fill the mentioned gap, we aimed to find whether ALS-derived crown metrics of width (WD), projection area (A_{2D}), volume (V), and surface area (A_{3D}) were affected by growth (Δ) and how relative growth ($r\Delta$) in the mentioned metrics differed between tree species groups in boreal forests. First, we demonstrated the feasibility of ALS data to detect individual tree crown growth over a 5-year monitoring period. The 3D crown metrics were more robust in detecting growth in comparison with 2D crown metrics. Considering the high correlation of crown metrics with the dbh and volume of trees, one of the possible applications of this study could be a large area estimation of tree growth allometry. Accurate estimates of crown growth could efficiently contribute in assessing forest responses to different thinning treatments, prescribed fire, fertilization, and other natural disturbances. In addition, the changes in crown growth provide information on forest health, productivity, and tree competition status. Second, a significant difference was achieved in the $r\Delta$ of Scots pine, Norway spruce, and birch, even though they had a little effect size. Scots pine was observed to have the highest $r\Delta$ and differed significantly relative to other tree species groups in $r\Delta_{WD}$, $r\Delta_{A_{2D}}$, $r\Delta_V$, and $r\Delta_{A_{3D}}$. Meanwhile, Norway spruce and birch showed no statistically significant difference in terms of $r\Delta_{WD}$, $r\Delta_V$, and $r\Delta_{A_{3D}}$. Our results confirmed the complex nature of growth with high variability in tree species groups, stimulating further attempts to investigate how controlling factors other than species can influence tree growth.

Author Contributions: Conceptualization and methodology, M.P., N.S. and V.K.; formal analysis, M.P.; funding and other resources, J.H. and M.V.; data curation, X.Y. and V.L.; writing—original draft preparation, M.P.; writing—review and editing, M.P., G.R., X.Y., V.L., J.H., N.S., V.K. and M.V.; visualization, M.P.; supervision, N.S., V.K. and M.V. All authors read and agreed to the published version of the manuscript.

Funding: This research was funded by the Academy of Finland. It was conducted as part of the Forest–Human–Machine Interplay flagship of science (decision number 337127), Density4Trees project (decision number 331711), and Scan4erstEcosystem Research Infrastructure (decision numbers 337810 and 346383).

Institutional Review Board Statement: Not applicable.

Informed Consent Statement: Not applicable.

Data Availability Statement: Not applicable.

Acknowledgments: The authors would like to thank Häme University of Applied Sciences for supporting the research activities in Evo.

Conflicts of Interest: The authors declare no conflict of interest.

References

- Peng, C.; Apps, M.J. Modelling the Response of Net Primary Productivity (NPP) of Boreal Forest Ecosystems to Changes in Climate and Fire Disturbance Regimes. *Ecol. Modell.* **1999**, *122*, 175–193. [[CrossRef](#)]
- Pretzsch, H. Growing Space and Competitive Situation of Individual Trees. In *Forest Dynamics, Growth and Yield*; Springer: Berlin/Heidelberg, Germany, 2009; pp. 291–336.
- Coops, N.C. Characterizing Forest Growth and Productivity Using Remotely Sensed Data. *Curr. For. Rep.* **2015**, *1*, 195–205. [[CrossRef](#)]
- Harris, N.L.; Gibbs, D.A.; Baccini, A.; Birdsey, R.A.; de Bruin, S.; Farina, M.; Fatoyinbo, L.; Hansen, M.C.; Herold, M.; Houghton, R.A.; et al. Global Maps of Twenty-First Century Forest Carbon Fluxes. *Nat. Clim. Chang.* **2021**, *11*, 234–240. [[CrossRef](#)]
- Wensel, L.C.; Meerschaert, W.J.; Biging, G.S. Tree Height and Diameter Growth Models for Northern California Conifers. *Hilgardia* **1987**, *55*, 1–20. [[CrossRef](#)]
- Weiskittel, A.R.; Hann, D.W.; Kershaw Jr, J.A.; Vanclay, J.K. *Forest Growth and Yield Modeling*; John Wiley & Sons: New York, NY, USA, 2011.
- Tompalski, P.; Coops, N.; White, J.; Wulder, M. Enhancing Forest Growth and Yield Predictions with Airborne Laser Scanning Data: Increasing Spatial Detail and Optimizing Yield Curve Selection through Template Matching. *Forests* **2016**, *7*, 255. [[CrossRef](#)]
- Munro, D.D. Growth Models for Tree and Stand Simulation. *For. Res.* **1974**, *30*, 7–21.
- Peng, C. Growth and Yield Models for Uneven-Aged Stands: Past, Present and Future. *For. Ecol. Manag.* **2000**, *132*, 259–279. [[CrossRef](#)]
- Jimenez-Perez, J.; Aguirre-Calderon, O.; Kramer, H. Tree Crown Structure Indicators in a Natural Uneven-Aged Mixed Coniferous Forest in Northeastern Mexico. In *Monitoring Science and Technology Symposium: Unifying Knowledge for Sustainability in the Western Hemisphere Proceedings RMRS-P-42CD*; Aguirre-Bravo, C., Pellicane, P.J., Burns, D.P., Draggan, S., Eds.; US Department of Agriculture, Forest Service, Rocky Mountain Research Station: Fort Collins, CO, USA, 2006; Volume 42, pp. 649–654.
- Biging, G.S.; Dobbertin, M. Evaluation of Competition Indices in Individual Tree Growth Models. *For. Sci.* **1995**, *41*, 360–377.
- Perin, J.; Hébert, J.; Brostaux, Y.; Lejeune, P.; Claessens, H. Modelling the Top-Height Growth and Site Index of Norway Spruce in Southern Belgium. *For. Ecol. Manag.* **2013**, *298*, 62–70. [[CrossRef](#)]
- Socha, J.; Pierzchalski, M.; Bałazy, R.; Ciesielski, M. Modelling Top Height Growth and Site Index Using Repeated Laser Scanning Data. *For. Ecol. Manag.* **2017**, *406*, 307–317. [[CrossRef](#)]
- Wulder, M.A.; Franklin, S.E. (Eds.) *Remote Sensing of Forest Environments: Concepts and Case Studies*; Springer: Berlin/Heidelberg, Germany, 2012; ISBN 978-1-4613-5014-9.
- Coops, N.C.; Hilker, T.; Wulder, M.A.; St-Onge, B.; Newnham, G.; Siggins, A.; Trofymow, J.A. Estimating Canopy Structure of Douglas-Fir Forest Stands from Discrete-Return LiDAR. *Trees* **2007**, *21*, 295. [[CrossRef](#)]
- Hyyppä, J.; Hyyppä, H.; Leckie, D.; Gougeon, F.; Yu, X.; Maltamo, M. Review of Methods of Small-footprint Airborne Laser Scanning for Extracting Forest Inventory Data in Boreal Forests. *Int. J. Remote Sens.* **2008**, *29*, 1339–1366. [[CrossRef](#)]
- García, M.; Saatchi, S.; Casas, A.; Koltunov, A.; Ustin, S.; Ramirez, C.; Balzter, H. Extrapolating Forest Canopy Fuel Properties in the California Rim Fire by Combining Airborne LiDAR and Landsat OLI Data. *Remote Sens.* **2017**, *9*, 394. [[CrossRef](#)]
- Kruper, A.; McGaughey, R.J.; Crumrine, S.; Bormann, B.T.; Bennett, K.; Bobsin, C.R. Using Airborne LiDAR to Map Red Alder in the Sappho Long-Term Ecosystem Productivity Study. *Remote Sens.* **2022**, *14*, 1591. [[CrossRef](#)]
- Réjou-Méchain, M.; Tymen, B.; Blanc, L.; Fauset, S.; Feldpausch, T.R.; Monteagudo, A.; Phillips, O.L.; Richard, H.; Chave, J. Using Repeated Small-Footprint LiDAR Acquisitions to Infer Spatial and Temporal Variations of a High-Biomass Neotropical Forest. *Remote Sens. Environ.* **2015**, *169*, 93–101. [[CrossRef](#)]

20. Cao, L.; Coops, N.C.; Innes, J.L.; Sheppard, S.R.J.; Fu, L.; Ruan, H.; She, G. Estimation of Forest Biomass Dynamics in Subtropical Forests Using Multi-Temporal Airborne LiDAR Data. *Remote Sens. Environ.* **2016**, *178*, 158–171. [[CrossRef](#)]
21. Tompalski, P.; Coops, N.; Marshall, P.; White, J.; Wulder, M.; Bailey, T. Combining Multi-Date Airborne Laser Scanning and Digital Aerial Photogrammetric Data for Forest Growth and Yield Modelling. *Remote Sens.* **2018**, *10*, 347. [[CrossRef](#)]
22. Vastaranta, M.; Yrttimaa, T.; Saarinen, N.; Yu, X.; Karjalainen, M.; Nurminen, K.; Karila, K.; Kankare, V.; Luoma, V.; Pyörälä, J.; et al. Airborne Laser Scanning Outperforms the Alternative 3D Techniques in Capturing Variation in Tree Height and Forest Density in Southern Boreal Forests. *Balt. For.* **2018**, *24*, 268–277.
23. Dassot, M.; Constant, T.; Fournier, M. The Use of Terrestrial LiDAR Technology in Forest Science: Application Fields, Benefits and Challenges. *Ann. For. Sci.* **2011**, *68*, 959–974. [[CrossRef](#)]
24. Gatzliolis, D.; Fried, J.S.; Monleon, V.S. Challenges to Estimating Tree Height via LiDAR in Closed-Canopy Forests: A Parable from Western Oregon. *For. Sci.* **2010**, *56*, 139–155.
25. Srinivasan, S.; Popescu, S.C.; Eriksson, M.; Sheridan, R.D.; Ku, N.W. Multi-Temporal Terrestrial Laser Scanning for Modeling Tree Biomass Change. *For. Ecol. Manag.* **2014**, *318*, 304–317. [[CrossRef](#)]
26. Holmgren, J.; Persson, Å. Identifying Species of Individual Trees Using Airborne Laser Scanner. *Remote Sens. Environ.* **2004**, *90*, 415–423. [[CrossRef](#)]
27. Popescu, S.C.; Zhao, K. A Voxel-Based Lidar Method for Estimating Crown Base Height for Deciduous and Pine Trees. *Remote Sens. Environ.* **2008**, *112*, 767–781. [[CrossRef](#)]
28. Kato, A.; Moskal, L.M.; Schiess, P.; Swanson, M.E.; Calhoun, D.; Stuetzle, W. Capturing Tree Crown Formation through Implicit Surface Reconstruction Using Airborne Lidar Data. *Remote Sens. Environ.* **2009**, *113*, 1148–1162. [[CrossRef](#)]
29. Duncanson, L.I.; Cook, B.D.; Hurtt, G.C.; Dubayah, R.O. An Efficient, Multi-Layered Crown Delineation Algorithm for Mapping Individual Tree Structure across Multiple Ecosystems. *Remote Sens. Environ.* **2014**, *154*, 378–386. [[CrossRef](#)]
30. Frew, M.S.; Evans, D.L.; Londo, H.A.; Cooke, W.H.; Irby, D. Measuring Douglas-Fir Crown Growth with Multitemporal LiDAR. *For. Sci.* **2016**, *62*, 200–212. [[CrossRef](#)]
31. Jung, S.-E.; Kwak, D.-A.; Park, T.; Lee, W.-K.; Yoo, S. Estimating Crown Variables of Individual Trees Using Airborne and Terrestrial Laser Scanners. *Remote Sens.* **2011**, *3*, 2346–2363. [[CrossRef](#)]
32. Londo, H.A. The Suitability of LiDAR-Derived Forest Attributes for Use in Individual-Tree Distance-Dependent Growth-and-Yield Modeling. Doctor of Philosophy, Mississippi State University, Mississippi State, MS, USA, 2010.
33. NASSET, E.; GOBAKKEN, T. Estimating Forest Growth Using Canopy Metrics Derived from Airborne Laser Scanner Data. *Remote Sens. Environ.* **2005**, *96*, 453–465. [[CrossRef](#)]
34. Yu, X.; Hyypä, J.; Kaartinen, H.; Maltamo, M.; Hyypä, H. Obtaining Plotwise Mean Height and Volume Growth in Boreal Forests Using Multi-temporal Laser Surveys and Various Change Detection Techniques. *Int. J. Remote Sens.* **2008**, *29*, 1367–1386. [[CrossRef](#)]
35. Dubayah, R.O.; Sheldon, S.L.; Clark, D.B.; Hofton, M.A.; Blair, J.B.; Hurtt, G.C.; Chazdon, R.L. Estimation of Tropical Forest Height and Biomass Dynamics Using Lidar Remote Sensing at La Selva, Costa Rica. *J. Geophys. Res. Biogeosciences* **2010**, *115*. [[CrossRef](#)]
36. Zhao, K.; Suarez, J.C.; Garcia, M.; Hu, T.; Wang, C.; Londo, A. Utility of Multitemporal Lidar for Forest and Carbon Monitoring: Tree Growth, Biomass Dynamics, and Carbon Flux. *Remote Sens. Environ.* **2018**, *204*, 883–897. [[CrossRef](#)]
37. Ma, Q.; Su, Y.; Tao, S.; Guo, Q. Quantifying Individual Tree Growth and Tree Competition Using Bi-Temporal Airborne Laser Scanning Data: A Case Study in the Sierra Nevada Mountains, California. *Int. J. Digit. Earth* **2018**, *11*, 485–503. [[CrossRef](#)]
38. Maltamo, M.; Vartiainen, P.; Packalen, P.; Korhonen, L. Estimation of Periodic Annual Increment of Tree Ring Widths by Airborne Laser Scanning. *Can. J. For. Res.* **2022**, *52*, 644–651. [[CrossRef](#)]
39. Duncanson, L.; Dubayah, R. Monitoring Individual Tree-based Change with Airborne Lidar. *Ecol. Evol.* **2018**, *8*, 5079–5089. [[CrossRef](#)] [[PubMed](#)]
40. COOMES, D.A.; ALLEN, R.B. Effects of Size, Competition and Altitude on Tree Growth. *J. Ecol.* **2007**, *95*, 1084–1097. [[CrossRef](#)]
41. Stephenson, N.L.; Das, A.J.; Condit, R.; Russo, S.E.; Baker, P.J.; Beckman, N.G.; Coomes, D.A.; Lines, E.R.; Morris, W.K.; Rüger, N.; et al. Rate of Tree Carbon Accumulation Increases Continuously with Tree Size. *Nature* **2014**, *507*, 90–93. [[CrossRef](#)] [[PubMed](#)]
42. Yu, X.; Hyypä, J.; Karjalainen, M.; Nurminen, K.; Karila, K.; Vastaranta, M.; Kankare, V.; Kaartinen, H.; Holopainen, M.; Honkavaara, E.; et al. Comparison of Laser and Stereo Optical, SAR and InSAR Point Clouds from Air- and Space-Borne Sources in the Retrieval of Forest Inventory Attributes. *Remote Sens.* **2015**, *7*, 15933–15954. [[CrossRef](#)]
43. Laasasenaho, J. Taper Curve and Volume Functions for Pine, Spruce and Birch. *Commun. Inst. For. Fenn.* **1982**, *108*, 1–74.
44. Axelsson, P. DEM Generation from Laser Scanner Data Using Adaptive TIN Models. *Int. Arch. Photogramm. Remote Sens. Spat.* **2000**, *33*, 110–117.
45. Isenburg, M. Use Buffers When Processing LiDAR in Tiles. Available online: <https://rapidlasso.com/2015/08/07/use-buffers-when-processing-lidar-in-tiles/> (accessed on 27 September 2022).
46. Khosravipour, A.; Skidmore, A.K.; Isenburg, M. Generating Spike-Free Digital Surface Models Using LiDAR Raw Point Clouds: A New Approach for Forestry Applications. *Int. J. Appl. Earth Obs. Geoinf.* **2016**, *52*, 104–114. [[CrossRef](#)]
47. Isenburg, M. Rasterizing Perfect Canopy Height Models from LiDAR. Available online: <https://rapidlasso.com/2014/11/04/rasterizing-perfect-canopy-height-models-from-lidar/> (accessed on 27 September 2022).

48. Roussel, J.R.; Auty, D. LidR: Airborne LiDAR Data Manipulation and Visualization for Forestry Applications. 2018. Available online: <https://cran.r-project.org/web/packages/lidR/index.html> (accessed on 27 September 2022).
49. Meyer, F.; Beucher, S. Morphological Segmentation. *J. Vis. Commun. Image Represent.* **1990**, *1*, 21–46. [[CrossRef](#)]
50. Næsset, E. Predicting Forest Stand Characteristics with Airborne Scanning Laser Using a Practical Two-Stage Procedure and Field Data. *Remote Sens. Environ.* **2002**, *80*, 88–99. [[CrossRef](#)]
51. Tompalski, P.; Coops, N.C.; White, J.C.; Goodbody, T.R.H.; Hennigar, C.R.; Wulder, M.A.; Socha, J.; Woods, M.E. Estimating Changes in Forest Attributes and Enhancing Growth Projections: A Review of Existing Approaches and Future Directions Using Airborne 3D Point Cloud Data. *Curr. For. Rep.* **2021**, *7*, 1–24. [[CrossRef](#)]
52. Yu, X.; Hyypä, J.; Kaartinen, H.; Maltamo, M. Automatic Detection of Harvested Trees and Determination of Forest Growth Using Airborne Laser Scanning. *Remote Sens. Environ.* **2004**, *90*, 451–462. [[CrossRef](#)]
53. Pyörälä, J.; Saarinen, N.; Kankare, V.; Coops, N.C.; Liang, X.; Wang, Y.; Holopainen, M.; Hyypä, J.; Vastaranta, M. Variability of Wood Properties Using Airborne and Terrestrial Laser Scanning. *Remote Sens. Environ.* **2019**, *235*, 111474. [[CrossRef](#)]
54. ESRI Spatial Join (Analysis). Available online: <https://pro.arcgis.com/en/pro-app/latest/tool-reference/analysis/spatial-join.htm> (accessed on 27 September 2022).
55. Vastaranta, M.; Holopainen, M.; Yu, X.; Hyypä, J.; Mäkinen, A.; Rasinmäki, J.; Melkas, T.; Kaartinen, H.; Hyypä, H. Effects of Individual Tree Detection Error Sources on Forest Management Planning Calculations. *Remote Sens.* **2011**, *3*, 1614–1626. [[CrossRef](#)]
56. Jakubowski, M.; Li, W.; Guo, Q.; Kelly, M. Delineating Individual Trees from Lidar Data: A Comparison of Vector- and Raster-Based Segmentation Approaches. *Remote Sens.* **2013**, *5*, 4163–4186. [[CrossRef](#)]
57. Zimmerman, D.W. A Note on the Influence of Outliers on Parametric and Nonparametric Tests. *J. Gen. Psychol.* **1994**, *121*, 391–401. [[CrossRef](#)]
58. Fernández-Sarría, A.; Martínez, L.; Velázquez-Martí, B.; Sajdak, M.; Estornell, J.; Recio, J.A. Different Methodologies for Calculating Crown Volumes of Platanus Hispanica Trees Using Terrestrial Laser Scanner and a Comparison with Classical Dendrometric Measurements. *Comput. Electron. Agric.* **2013**, *90*, 176–185. [[CrossRef](#)]
59. Yrttimaa, T.; Luoma, V.; Saarinen, N.; Kankare, V.; Junttila, S.; Holopainen, M.; Hyypä, J.; Vastaranta, M. Monitoring Tree Growth Allometry Using Two-Date Terrestrial Laser Scanning. *SSRN Electron. J.* **2022**. [[CrossRef](#)]
60. Niemistö, P.; Kilpeläinen, H.; Poutiainen, E. Effect of First Thinning Type and Age on Growth, Stem Quality and Financial Performance of a Scots Pine Stand in Finland. *Silva Fenn.* **2018**, *52*, 21. [[CrossRef](#)]
61. Pommerening, A.; Muszta, A. Methods of Modelling Relative Growth Rate. *For. Ecosyst.* **2015**, *2*, 5. [[CrossRef](#)]
62. Kim, T.K.; Park, J.H. More about the Basic Assumptions of T-Test: Normality and Sample Size. *Korean J. Anesthesiol.* **2019**, *72*, 331–335. [[CrossRef](#)]
63. Triola, M.F.; Goodman, W.M.; Law, R.; Labute, G. *Elementary Statistics*, 13th ed.; Pearson/Addison-Wesley Reading: Boston, FL, USA, 2006.
64. Olejnik, S.; Algina, J. Generalized Eta and Omega Squared Statistics: Measures of Effect Size for Some Common Research Designs. *Psychol. Methods* **2003**, *8*, 434–447. [[CrossRef](#)]
65. Cohen, J. *Statistical Power Analysis for the Behavioral Sciences*; Routledge: New York, NY, USA, 2013.
66. Kwak, D.A.; Lee, W.K.; Cho, H.K.; Lee, S.H.; Son, Y.; Kafatos, M.; Kim, S.R. Estimating Stem Volume and Biomass of Pinus Koraiensis Using LiDAR Data. *J. Plant Res.* **2010**, *123*, 421–432. [[CrossRef](#)]
67. Getzin, S.; Wiegand, K. Asymmetric Tree Growth at the Stand Level: Random Crown Patterns and the Response to Slope. *For. Ecol. Manag.* **2007**, *242*, 165–174. [[CrossRef](#)]
68. Vepakomma, U.; St-Onge, B.; Kneeshaw, D. Response of a Boreal Forest to Canopy Opening: Assessing Vertical and Lateral Tree Growth with Multi-Temporal Lidar Data. *Ecol. Appl.* **2011**, *21*, 99–121. [[CrossRef](#)] [[PubMed](#)]
69. Rapp, J.M.; Silman, M.R.; Clark, J.S.; Girardin, C.A.J.; Galiano, D.; Tito, R. Intra- and Interspecific Tree Growth across a Long Altitudinal Gradient in the Peruvian Andes. *Ecology* **2012**, *93*, 2061–2072. [[CrossRef](#)] [[PubMed](#)]
70. Kaitaniemi, P.; Lintunen, A. Neighbor Identity and Competition Influence Tree Growth in Scots Pine, Siberian Larch, and Silver Birch. *Ann. For. Sci.* **2010**, *67*, 604. [[CrossRef](#)]
71. Aakala, T.; Fraver, S.; D’Amato, A.W.; Palik, B.J. Influence of Competition and Age on Tree Growth in Structurally Complex Old-Growth Forests in Northern Minnesota, USA. *For. Ecol. Manag.* **2013**, *308*, 128–135. [[CrossRef](#)]
72. Popescu, S.C.; Wynne, R.H. Seeing the Trees in the Forest. *Photogramm. Eng. Remote Sens.* **2004**, *70*, 589–604. [[CrossRef](#)]
73. Shan, J.; Toth, C.K. Topographic Laser Ranging and Scanning: Principles and Processing. In *Topographic Laser Ranging and Scanning*; CRC Press: Boca Raton, FL, USA, 2017; pp. 1–590. [[CrossRef](#)]
74. Csanyi, N.; Toth, C.K. LiDAR Data Accuracy: The Impact of Pulse Repetition Rate. In Proceedings of the MAPPS/ASPRS 2006 Fall Conference, San Antonio, TX, USA, 6–10 November 2006.
75. Hudak, A.T.; Strand, E.K.; Vierling, L.A.; Byrne, J.C.; Eitel, J.U.H.; Martinuzzi, S.; Falkowski, M.J. Quantifying Aboveground Forest Carbon Pools and Fluxes from Repeat LiDAR Surveys. *Remote Sens. Environ.* **2012**, *123*, 25–40. [[CrossRef](#)]
76. Fekety, P.A.; Falkowski, M.J.; Hudak, A.T. Temporal Transferability of LiDAR-Based Imputation of Forest Inventory Attributes. *Can. J. For. Res.* **2015**, *45*, 422–435. [[CrossRef](#)]
77. Yu, X.; Hyypä, J.; Kukko, A.; Maltamo, M.; Kaartinen, H. Change Detection Techniques for Canopy Height Growth Measurements Using Airborne Laser Scanner Data. *Photogramm. Eng. Remote Sens.* **2006**, *72*, 1339–1348. [[CrossRef](#)]

-
78. Kaartinen, H.; Hyypä, J.; Yu, X.; Vastaranta, M.; Hyypä, H.; Kukko, A.; Holopainen, M.; Heipke, C.; Hirschmugl, M.; Morsdorf, F.; et al. An International Comparison of Individual Tree Detection and Extraction Using Airborne Laser Scanning. *Remote Sens.* **2012**, *4*, 950–974. [[CrossRef](#)]